NANO LETTERS

pubs.acs.org/NanoLett Letter

Adiabatic Frequency Conversion Using a Time-Varying Epsilon-Near-Zero Metasurface

Kai Pang,* M. Zahirul Alam, Yiyu Zhou, Cong Liu, Orad Reshef, Karapet Manukyan, Matt Voegtle, Anuj Pennathur, Cindy Tseng, Xinzhou Su, Hao Song, Zhe Zhao, Runzhou Zhang, Haoqian Song, Nanzhe Hu, Ahmed Almaiman, Jahan M. Dawlaty, Robert W. Boyd, Moshe Tur, and Alan E. Willner

Cite This: *Nano Lett.* 2021, 21, 5907−5913 Read Online

ACCESS | Metrics & More | Article Recommendations

ABSTRACT: A time-dependent change in the refractive index of a material leads to a change in the frequency of an optical beam passing through that medium. Here, we experimentally demonstrate that this effect—known as adiabatic frequency conversion (AFC)—can be significantly enhanced by a nonlinear epsilon-near-zero-based (ENZ-based) plasmonic metasurface. Specifically, by using a 63-nm-thick metasurface, we demonstrate a large, tunable, and broadband frequency shift of up to ∼11.2 THz with a pump intensity of 4 GW/cm^2. Our results represent a decrease of ∼10 times in device thickness and 120 times in pump peak intensity compared with the cases of bare, thicker ENZ materials for the similar amount of frequency shift. Our findings might potentially provide insights for designing efficient time-varying metasurfaces for the manipulation of ultrafast pulses.

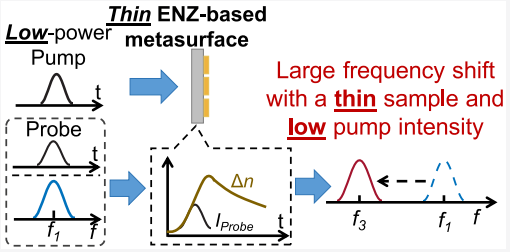

KEYWORDS: *epsilon-near-zero metasurface, nonlinear optical materials, indium−tin oxide, time-varying refractive index, dynamic resonance, nonlinear frequency shift*

INTRODUCTION

Optical frequency conversion techniques have potential applications in optical communication, signal processing, imaging, and quantum information processing.[1−3] One example of frequency conversion techniques is adiabatic frequency conversion (AFC), which potentially enables continuous shift of the carrier frequency of a beam without phase-matching considerations.[4−6] Generally, AFC can be implemented by letting a light beam pass through a medium that exhibits a time-varying refractive index (Figure 1a). The sign and the magnitude of the carrier frequency shift depend on the sign and the speed of the change in the refractive index, i.e., the rate of the change in the phase shift.[4,7−9]

Previously, a number of different techniques have been investigated to implement time-varying media to demonstrate AFC.[4−6,10−24] However, in many previous implementations, the possible frequency shift is limited by the weaker nonlinear response of a typical optical material. In recent years, epsilon-near-zero (ENZ) materials have gained much interest because of their potential unusual linear optical behaviors and large nonlinearity.[25−29] Particularly, a transparent conducting oxide-based ENZ thin film is reported to exhibit optically induced unity-order changes in the refractive index in subpicosecond time scales.[26] Because of the near-zero linear refractive index and a large possible nonlinear change in refractive index, an ENZ medium could potentially provide a natural platform for a large AFC. For example, (i) an ∼8.8 THz redshift of the carrier frequency was observed with a pump peak power intensity of 770 GW/cm^2 using a 500-nm-thick aluminum-doped zinc oxide-based ENZ film;[30] (ii) in addition, by using a 620-nm-thick indium−tin oxide-based (ITO-based) ENZ film, a tunable redshift of up to ∼11.1 THz was achieved with a 483-GW/cm^2 pump peak intensity.[7]

Although the nonlinear response of the ENZ material is large, a significantly stronger nonlinear response can be engineered by introducing nanostructures on an ENZ film. One possible nanostructure is a gold plasmonic antenna array.[31] It was reported that an ENZ-based nanoantenna metasurface exhibits a broadband and large nonlinear response because of strong coupling between the plasmonic mode of the antenna and the ENZ mode of the ITO thin film.[31] Compared with a bare ENZ film, such a device not only exhibits a larger change in the refractive index but also significantly lowers the operating power (i.e., pump peak intensity).

Recently, a self-phase-modulation-induced frequency shift was demonstrated using a 92-nm-thick ENZ-based metasur-

Received: February 7, 2021
Revised: July 4, 2021
Published: July 12, 2021

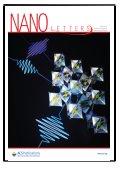

https://doi.org/10.1021/acs.nanolett.1c00550
Nano Lett. 2021, 21, 5907−5913

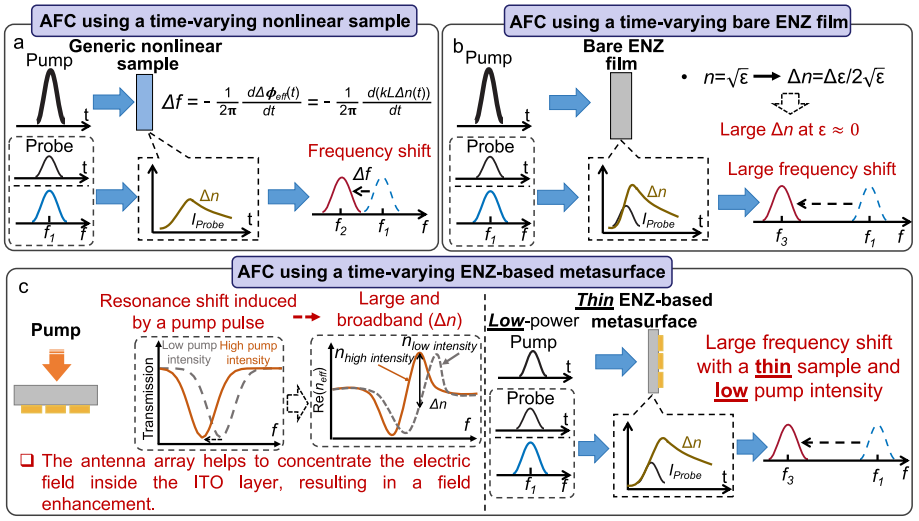

Figure 1. Basic concept of AFC. (a) An optical pump pulse can induce a time-varying change in the refractive index of a medium. A probe pulse traveling through the same medium experiences a time-dependent phase shift ($\Delta\phi_{eff}$), resulting in an adiabatic frequency shift of the probe pulse that is proportional to the rate of the change in the refractive index (Δn). L is the thickness of the nonlinear sample in this figure. (b) A thick bare ENZ ($\varepsilon \approx 0$) film under pulsed optical excitation can be used for AFC by exploiting the unity-order change in the refractive index of the film. (c) An engineered plasmonic metasurface incorporating an ENZ thin film exhibits a larger nonlinear optical response compared to that of a bare ENZ film. Such a metasurface exhibits a large change in the effective refractive index (Δn_{eff}) due to the time-varying change in the resonance frequency. In addition, the antenna array also helps to concentrate the incident electric field inside the ENZ layer, resulting in a field enhancement. Consequently, a thinner ENZ-based metasurface can be utilized to achieve a large AFC with a low pump intensity. $k = 2\pi/\lambda$ is the wavenumber.

face.[32] In that work, it was reported that a near-resonant high-intensity input pulse propagating through an ENZ-based metasurface experiences a frequency shift of ∼1.6 THz due to a time-dependent change in the optical path length due to the self-action nonlinear optical effect. However, a single-beam operation might not fully exploit the time-dependent nature of such a system. In contrast to this previous report, a pump−probe scheme allows additional control of the frequency shift of the probe beam as a function of pump intensity and the pump−probe delay time and thus leads to a significantly larger frequency shift compared to a single-beam operation.[33] Here we show a pump-induced change in the frequency of a probe beam due to the dynamic variations of the effective refractive index of the metasurface in the presence of the pump beam. As a result, the probe experiences a time-dependent phase shift ($\Delta\phi_{eff}$). The magnitude of the phase shift depends on both the intensity of the pump beam and the relative time delay between the pump and the probe, leading to a tunable frequency shift of the probe (Figure 1a). Additionally, because of weak-wave retardation effects, a pump can impart a larger phase shift to a weak probe than to itself.[1] Consequently, the pump-induced change in the frequency can potentially be larger compared to the single-beam study.[32] Moreover, because the refractive index change is induced by the pump, the frequency shift of the probe pulse may now be independently controlled by the pump intensity and the pump−probe delay time.

Here we demonstrate a large, tunable, and broadband frequency shift of up to ∼11.2 THz with a 4-GW/cm^2 pump intensity using a 63-nm-thick ENZ-based metasurface. Our results represent a decrease of ∼10 times in device thickness and 120 times in pump peak intensity compared with the cases of bare, thicker ENZ materials for the similar amount of frequency shift.[7,30] In addition, this also represents a ∼7 times larger frequency shift with a thinner device and a similar pump peak intensity, when compared to previous ENZ-based metasurface work.[32] Moreover, we see that the magnitude of the frequency shift depends on—and thus can be controlled by—both the pump−probe delay time and the pump peak intensity. Furthermore, the AFC was demonstrated in a broadband wavelength range from 1257 to 1404 nm.

RESULTS AND DISCUSSION

Concept of AFC Using ENZ-Based Metasurface. A bare ENZ film has been reported to exhibit a large Δn in subpicosecond time scales in the ENZ region (i.e., $\varepsilon \approx 0$).[26] This is mainly due to two reasons: (i) the free-electron heat capacity of the ENZ film is relatively low, leading to a large change in the free-electron temperature and thus a large change in its permittivity; (ii) on the basis of the formula $\Delta n = \Delta\varepsilon/2\sqrt{\varepsilon}$, Δn is relatively larger at the ENZ region for a given $\Delta\varepsilon$. Therefore, a bare ENZ film can potentially be used as a platform to achieve a large AFC (Figure 1b).[7,30]

However, the optical nonlinearity of the ENZ film can be further enhanced by introducing a gold plasmonic antenna array onto an ENZ film.[31] In this ENZ-based metasurface, the plasmonic antenna array plays three crucial roles: (i) It allows for efficient coupling of the free-space radiation into the ITO layer. (ii) The antenna array helps to concentrate the electric field inside the ENZ layer, resulting in a field enhancement that lowers the nonlinear intensity threshold. (iii) Because of the strong coupling between the antenna array and the ENZ film, the electric near field of each antenna is pulled into the thin ENZ substrate. Consequently, the resonance condition of the hybrid system has a strong dependence on the refractive index of the subwavelength-thick ENZ substrate.[31] When an optical pulse passes through the metasurface, the ENZ film exhibits a relatively higher change in refractive index due to its large nonlinear response, which leads to a larger resonance shift for this metasurface[26,31] (Figure 1c). As a result, the overall change in the effective refractive index (i.e., Δn_{eff}) is significantly enhanced in a broadband range. Thus, the AFC effect resulting

https://doi.org/10.1021/acs.nanolett.1c00550
Nano Lett. 2021, 21, 5907−5913

from a time-varying change in the resonance condition of the strongly coupled system is enhanced. We note that Δn_{eff} of the coupled system depends on the Q-factor of the resonator and the coupling dynamics between the antennas and the ENZ film, which can be computed using homogenization techniques.[31,34]

Linear Optical Response of the Metasurface. ITO is a transparent conducting oxide, and it generally exhibits zero real permittivity in the near-IR spectral range. Figure 2a shows the complex permittivity values of the ITO film we used for this work, which is obtained using spectroscopic ellipsometry. It is observed that the 23-nm-thick ITO film has zero real permittivity at 1420 nm. Generally, a thin ITO-based ENZ film exhibits a nonpropagating surface mode known as the ENZ mode.[31,35,36] The dispersion of the ENZ mode depends on the thickness of the ITO layer and affects the field enhancement.[35] Typically the field enhancement, due to the excitation of the ENZ mode, is maximized for a deeply subwavelength thin film. In this study we choose a commercially available 23-nm-thick ITO film as the ENZ substrate. A similar substrate was previously used to demonstrate a broadband and large nonlinear response.[31] When a plasmonic antenna array with a fundamental resonance wavelength close to the zero-permittivity wavelength is placed on the ITO layer, the plasmonic mode of the antenna and the ENZ mode of the ITO layer interact with each other.[31,35−37] This results in a strong-coupling-induced spectral splitting of the plasmonic resonance of the antenna array. Figures 2b presents the finite-difference-time-domain (FDTD) simulation of transmittance for the ENZ-based metasurface with various antenna lengths. We find that the positions of the two resonance dips are dependent on the antenna length. The existence of a spectral anticrossing is a signature of the strong coupling regime between the antennas and the ITO film. Typically, the low-frequency hybrid resonance is the symmetric mode, and the high-frequency one is antisymmetric. We note that the linear responses of such metasurfaces have been discussed in a number of references.[36,38−40] Panels c and d of Figure 2 show the 3D schematic and the SEM image of metasurface we used in this study, respectively. We measure the linear transmission spectrum of the metasurface using a white light source (Figure 2e). The experimentally measured linear transmission spectrum of the metasurface exhibits two distinct dips—centered at ∼1200 nm and at ∼1550 nm—confirming the strong coupling effects. We note that the simulation and experimental results of the linear transmission are close, and the disagreements might be caused by various fabrication and alignment imperfections. We also note that in the absence of the ITO layer between gold antenna array and the substrate, the resonance dip of the transmission spectrum is at ∼1290 nm. Figure 2f shows FDTD simulation results of the electric field distribution of the coupled structure. A large field enhancement is observed which is caused by the near-field interactions between the ITO film and the antenna array. We perform a series of degenerate pump−probe measurements for this metasurface as functions of pump intensities, pump−probe delay, and carrier central frequency to investigate the AFC effect.

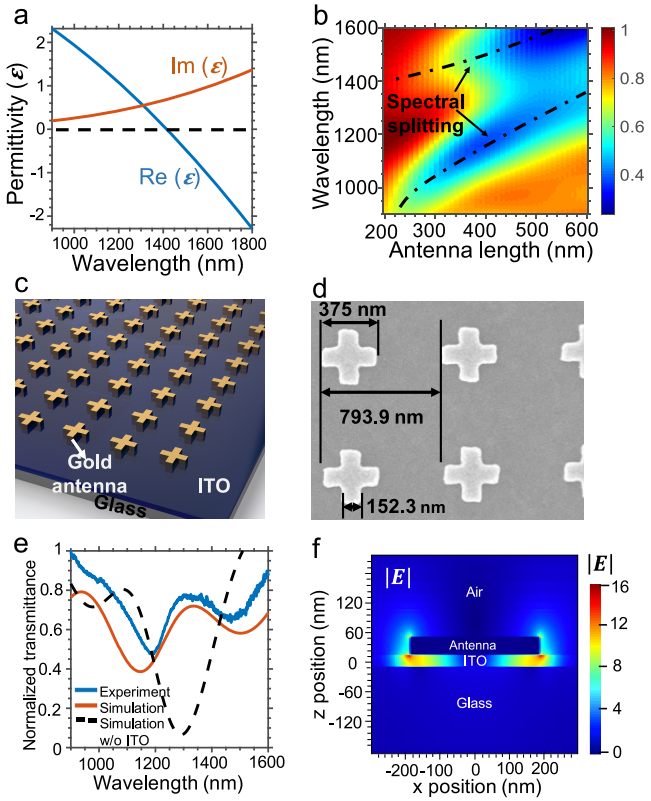

Figure 2. (a) Measured real and imaginary parts of the permittivity of an ITO film. (b) FDTD simulation results of the transmittance of the ENZ-based metasurface with various antenna lengths. (c) Basic structure of the ENZ-based metasurface device. The ITO thickness is 23 nm, and the gold antenna thickness is 40 nm. (d) Scanning electron micrograph of the fabricated gold antenna array. (e) Simulated and experimental results for the linear response of the metasurface exhibiting strong coupling-induced resonance splitting larger than the line width of the antenna resonances in the presence of the ENZ substrate. (f) FDTD simulation results of the enhanced electric field distribution of the coupled structure at an input wavelength of 1304 nm with the light polarized along the horizontal (x) axis of the antenna.

AFC Measurement at 1304 nm. First, we experimentally measured the probe spectra for various pump−probe delay times and different pump peak intensities when both pump and probe wavelengths are at ∼1304 nm (Figure 3a−c). We first choose this wavelength as an example to show the transmission spectra because this is nearly equidistant from the two main resonances of the metasurface based on the linear measurement in Figure 2e. Two other wavelengths will be also explored in the next section. We observe that the probe's transmitted spectra exhibit red-shifted peaks. This is because the probe beam mainly experiences a rise of the refractive index in the metasurface when the sign of n_2 is positive. In addition, we see that the probe's spectral redshift increases with a decreasing pump−probe delay for a given pump intensity. Here, the measured blueshift of the probe beam is not apparent, when the pump peak intensity is relatively low. This observation is different from reported red- and blue-shifted peaks, based on the different pump−probe delay, in previous ENZ-based AFC experiments.[7] We attribute this to the relatively slow decay time (∼500 fs) of the refractive index of such a metasurface compared to the probe's temporal duration (∼50 fs).[31] Compared with the bare ITO film, the decay time of the ENZ-based metasurface is relatively longer. This might be attributed to the low-Q resonance of the coupled system, modified electron−electron and electron−phonon scattering rate, and electron−phonon coupling

https://doi.org/10.1021/acs.nanolett.1c00550
Nano Lett. 2021, 21, 5907−5913

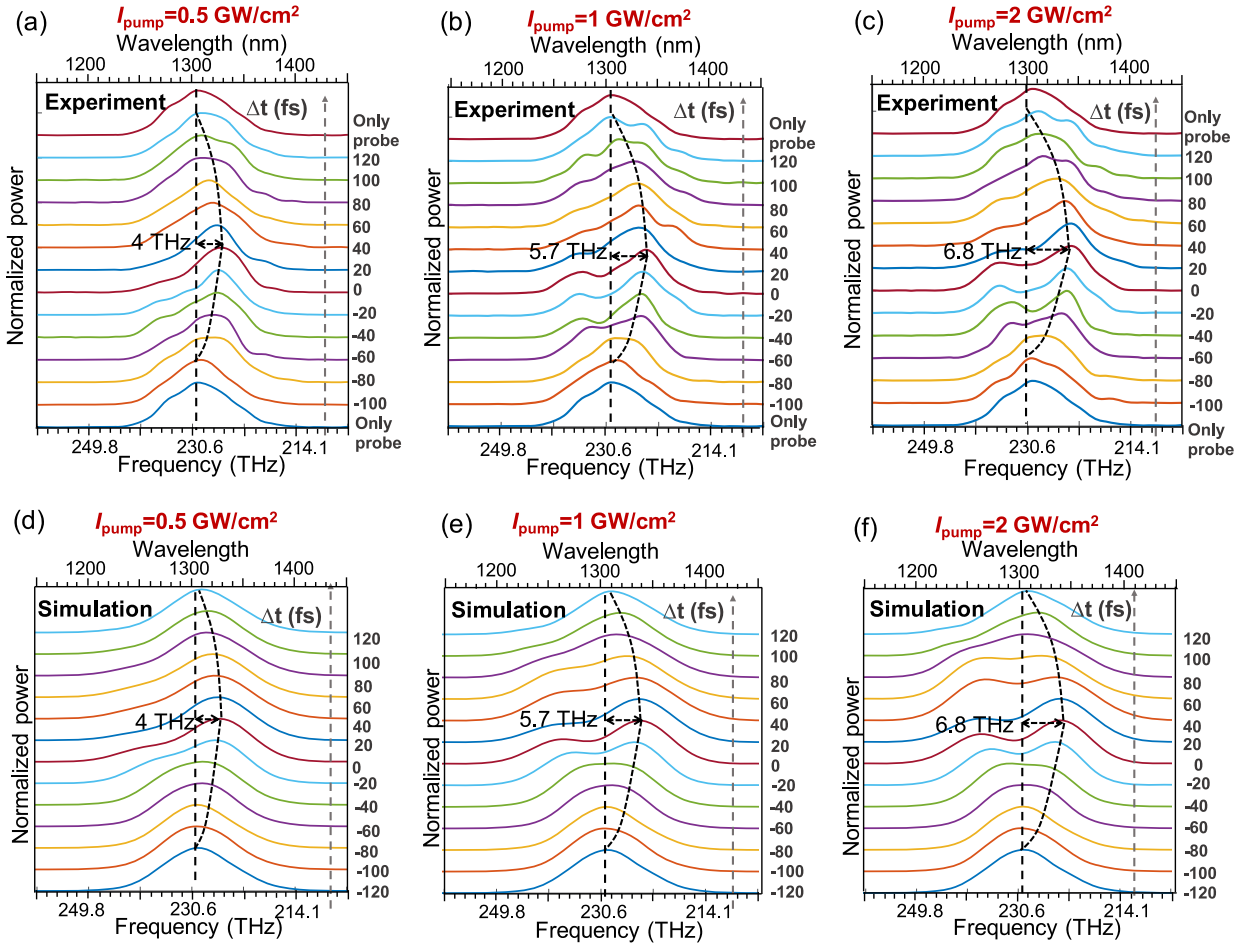

Figure 3. Experimental and simulated probe spectra at λ_0 = 1304 nm. (a–c) Normalized experimental probe spectra as a function of pump–probe delay times with various pump peak intensities. (d–f) Corresponding numerically simulated probe spectra by FDTD models.

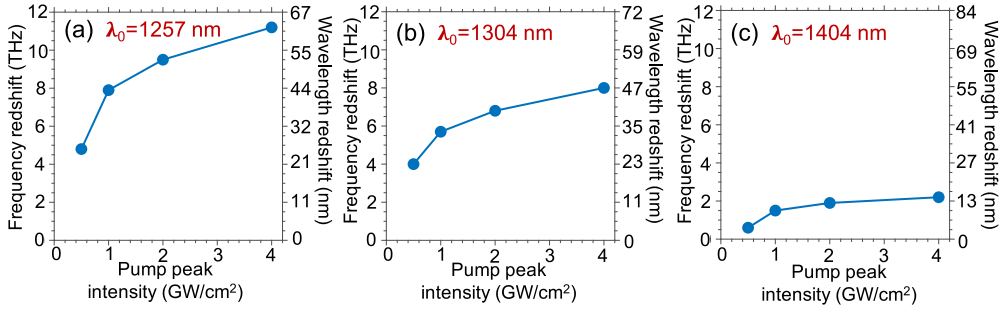

Figure 4. Frequency shifts at different central wavelengths. (a–c) Experimentally measured frequency shifts with various pump peak intensities for different central wavelengths (1257, 1304, and 1404 nm).

coefficient due to the presence of the gold nano structures.[31] Moreover, we find that for a given pump–probe delay, the spectral shift's magnitude increases with the increase in the pump intensity. This is because a higher-intensity pump induces a larger refractive index change, leading to a larger spectral shift. Furthermore, we see that as the pump intensity increases, another peak occurs at the left side of the probe spectra near zero delay time. Because the optical thickness of the metasurface is smaller than the longitudinal length of the probe, a part of the probe's energy might not reside inside the metasurface at a given instant of time. Consequently, not all energy of the probe is frequency shifted by the same amount. This leads to an observation of the blueshifted peaks with increasing pump intensity for a given pump–probe delay.[7]

To investigate the underlying mechanisms numerically, we perform a series of FDTD simulations. We model the nonlinear optical response of ITO with an effective delayed third-order nonlinearity. Here, we make a number of assumptions: (i) We attribute the nonlinearity only to the ITO layer, and we consider the gold to be a linear material. Generally, the nonlinearity of gold is primarily caused by intraband effects for the wavelengths of interest in this study.[41] The third-order susceptibility $\chi^{(3)}$ of gold induced by intraband effects at these wavelengths are on the order of 10^{-19} m^2/V^2, which is a few orders of magnitude smaller than the effective

https://doi.org/10.1021/acs.nanolett.1c00550
Nano Lett. 2021, 21, 5907–5913

$\chi^{(3)}$ of ITO used in the simulation (10^{-16}m^2/V^2).[41] (ii) We take the effective values of $\chi^{(3)}$ of ITO to be purely real, because we are interested in the frequency shift here. (iii) We take the saturation due to higher-order nonlinear effects into account implicitly by choosing effective $\chi^{(3)}$ values that decrease with increasing pump intensities. We find that the effective $\chi^{(3)}$ value for the case of the highest pump intensity is approximately a factor of 2 smaller than that for the lowest intensity. Our simulation reproduces the main experimental observations, namely that the magnitude of the probe frequency shift is a function of pump intensity and the temporal pump−probe delay.

Broadband Response. To investigate the bandwidth of the observed effect, we repeated the above measurements for two other wavelengths, 1257 and 1404 nm. Figure 4 summarizes our observations for all measurements. We observe a similar trend for all three wavelengths: the frequency redshift increases with increasing pump intensities for a given pump−probe delay. Moreover, the probe's frequency shift for a given pump intensity and delay decreases with an increase of the pump's wavelength. This observation is consistent with previous reports that the nonlinear response of an ITO-antenna coupled metasurface decreases with increasing detuning from the resonance.[31] Furthermore, we observe a change in the probe frequency of 11.2 THz when both pump and probe are at 1257 nm with a pump peak intensity of 4 GW/cm^2, which is similar to that of previous reports.[7,30]

CONCLUSION

In summary, we have experimentally demonstrated a large, tunable, and broadband AFC using a 63-nm-thick ENZ-based metasurface. Previous work has shown that large nonlinear optical responses can be engineered and enhanced by incorporating nanoantenna with the ENZ material.[31] In addition, it has also been demonstrated the AFC effect in a 620-nm-thick ENZ material.[7] Considering the understanding developed in two previous contributions, we demonstrate here that the AFC effect in a 63-nm-thick ENZ-based metasurface can be as large as what can be achieved in a 620-nm-thick ENZ material using more than 2 orders of magnitude lower pump intensity. Moreover, in comparison to recent work on self-induced frequency conversion,[32] we (a) show seven times larger frequency shifts, (b) provide evidence of the broadband nature of the process, and (c) demonstrate an additional route to tunability using pump−probe delay. Our findings might potentially provide insights into designing time-varying metasurfaces for the manipulation of ultrafast pulses. We note that a time-varying metasurface that can change the frequency of a probe beam might be used, in conjunction with an optical filter, to implement a pump-induced nonreciprocal device. In addition, AFC effects may also find applications in signal processing for optical communications.[42−44]

It is worth mentioning the following points: (i) The frequency shift saturates when the pump peak intensity is around 4 GW/cm^2 because of the saturation of Δn. This might be induced by a large damping of the thin ITO, which limits the achievable temperature of the free electrons. In addition, the increased electron temperature spectrally widens the resonance of the coupled structure, limiting the achievable phase shift.[31] In order to further increase the frequency shift, one may consider cascading multiple ENZ-metasurfaces or placing such a metasurface inside a cavity. However, a higher power loss would be induced when using multiple metasurfaces. Potential methods to reduce the power loss might include the use of dielectric nanoantennas and an ENZ material with less absorption. (ii) The antenna array geometry is chosen to be cross-shaped in both the simulation and the experiments such that there is little polarization dependence on the linear or nonlinear response.[32] In this work, we present experimental results only when both the pump and the probe are aligned with one of the principal axes of the metasurface. It should be noted that the nonlinear response of the cross-shaped antenna coupled to the ENZ medium is rotation-invariant as long as both the pump and the probe have the same polarization. However, if their polarization states are not the same, the resulting frequency shift might be lower, because the pump beam will induce a smaller refractive index change in the direction of the probe polarization. (iii) The frequency-dependent nonlinear properties of the ENZ-based metasurface can be potentially tailored by engineering the shapes and various geometric parameters of the antenna and by controlling the free-electron density and thickness of the ENZ layer. Therefore, the platform presented in this work might be potentially tailored to achieve AFC or some other applications in another central frequency.

METHODS

Fabrication. The 500 μm × 500 μm antenna array was fabricated on commercially available ITO on glass substrates (PGO GmbH). The antenna patterns were defined in a bilayer poly (methyl-methacrylate) resist using electron beam lithography (Raith Pioneer 30 kV), followed by Au deposition and a liftoff step. Intraparticle proximity error correction was used to ensure sharp corners and a good cross shape of the antennas.

Experimental Setup. An optical parametric amplifier pumped by a Ti:sapphire laser is used to generate optical pulses of ∼50 fs duration. The output beam is split into a pump and a probe using a pellicle beam splitter. In each arm, a half waveplate and a polarizer are used to control the power incident on the sample. The probe peak intensity is kept to 0.1 GW cm^{-2} to avoid inducing significant nonlinear effects. We use a mechanical delay stage to tune the delay time between pump and probe. Two lenses are then used to focus the pump and probe on the same spot of the metasurface with spot sizes of 65 and 25 μm, respectively. Because of the probe's smaller beam waist compared to the pump, the probe experiences nearly uniform pump intensity, i.e., uniform refractive index change in the transverse plane.

AUTHOR INFORMATION

Corresponding Author

Kai Pang − *Department of Electrical and Computer Engineering, University of Southern California, Los Angeles, California 90089, United States;* orcid.org/0000-0002-2405-7859; Email: kaipang@usc.edu

Authors

M. Zahirul Alam − *Department of Physics, University of Ottawa, Ottawa, Ontario, Canada*

Yiyu Zhou − *The Institute of Optics, University of Rochester, Rochester, New York 14627, United States*

Cong Liu − *Department of Electrical and Computer Engineering, University of Southern California, Los Angeles, California 90089, United States; Department of Physics and Astronomy, University of Southern California, Los Angeles,*

https://doi.org/10.1021/acs.nanolett.1c00550
Nano Lett. 2021, 21, 5907−5913

California 90089, United States; orcid.org/0000-0003-0089-0763
Orad Reshef − *Department of Physics, University of Ottawa, Ottawa, Ontario, Canada;* orcid.org/0000-0001-9818-8491
Karapet Manukyan − *Department of Electrical and Computer Engineering, University of Southern California, Los Angeles, California 90089, United States*
Matt Voegtle − *Department of Chemistry, University of Southern California, Los Angeles, California 90089, United States*
Anuj Pennathur − *Department of Chemistry, University of Southern California, Los Angeles, California 90089, United States*
Cindy Tseng − *Department of Chemistry, University of Southern California, Los Angeles, California 90089, United States*
Xinzhou Su − *Department of Electrical and Computer Engineering, University of Southern California, Los Angeles, California 90089, United States*
Hao Song − *Department of Electrical and Computer Engineering, University of Southern California, Los Angeles, California 90089, United States*
Zhe Zhao − *Department of Electrical and Computer Engineering, University of Southern California, Los Angeles, California 90089, United States*
Runzhou Zhang − *Department of Electrical and Computer Engineering, University of Southern California, Los Angeles, California 90089, United States*
Haoqian Song − *Department of Electrical and Computer Engineering, University of Southern California, Los Angeles, California 90089, United States*
Nanzhe Hu − *Department of Electrical and Computer Engineering, University of Southern California, Los Angeles, California 90089, United States*
Ahmed Almaiman − *Department of Electrical and Computer Engineering, University of Southern California, Los Angeles, California 90089, United States; King Saud University, Riyadh, Saudi Arabia*
Jahan M. Dawlaty − *Department of Chemistry, University of Southern California, Los Angeles, California 90089, United States;* orcid.org/0000-0001-5218-847X
Robert W. Boyd − *Department of Physics, University of Ottawa, Ottawa, Ontario, Canada; The Institute of Optics, University of Rochester, Rochester, New York 14627, United States;* orcid.org/0000-0002-1234-2265
Moshe Tur − *School of Electrical Engineering, Tel Aviv University, Tel Aviv 69978, Israel*
Alan E. Willner − *Department of Electrical and Computer Engineering, University of Southern California, Los Angeles, California 90089, United States*

Complete contact information is available at: https://pubs.acs.org/10.1021/acs.nanolett.1c00550

Author Contributions

M.Z.A., K.P., R.W.B., and A.E.W. conceived the work. M.Z.A., K.P., Y.Z., and O.R. designed the experiment. O.R. fabricated the metasurface. K.P. with help from M.Z.A., Y.Z., M.V., A.P., C.T., and X.S. performed laboratory measurements. K.P. with help from M.Z.A. and Y.Z. performed data analysis and developed the numerical model. K.P., M.Z.A., and Y.Z wrote the first draft. All authors contributed to the discussion of the results and the preparation of the final version of the manuscript. R.W.B. and A.E.W. supervised the work.

Notes

The authors declare no competing financial interest.

■ ACKNOWLEDGMENTS

This research was developed with funding from the Defense Advanced Research Projects Agency (DARPA) under the NLM Nascent Light-Matter Interactions program (Grant No. W911NF-18-0369). Fabrication in this work was performed in part at the Centre for Research in Photonics at the University of Ottawa (CRPuO). This research was undertaken thanks in part to funding from the Canada First Research Excellence Fund (CFREF) and the Canada Research Chairs (CRC) program. We acknowledge the support of the Natural Sciences and Engineering Research Council of Canada (NSERC) (funding reference number RGPIN/2017-06880). O.R. acknowledges the support of the Banting Postdoctoral Fellowship from NSERC. Qualcomm Innovation Fellowship (QIF).

■ REFERENCES

(1) Boyd, R. W. *Nonlinear optics*; Elsevier, 2020.
(2) Agrawal, G. *Nonlinear fiber optics*; Elsevier, 2019.
(3) Campagnola, P. J.; Dong, C.-Y. Second harmonic generation microscopy: principles and applications to disease diagnosis. *Laser Photonics Rev.* **2011**, *5*, 13−26.
(4) Preble, S. F.; Xu, Q.; Lipson, M. Changing the colour of light in a silicon resonator. *Nat. Photonics* **2007**, *1*, 293−296.
(5) Upham, J.; Tanaka, Y.; Asano, T.; Noda, S. On-the-fly wavelength conversion of photons by dynamic control of photonic waveguides. *Appl. Phys. Express* **2010**, *3*, 062001.
(6) Kampfrath, T.; Beggs, D. M.; White, T. P.; Melloni, A.; Krauss, T. F.; Kuipers, L. Ultrafast adiabatic manipulation of slow light in a photonic crystal. *Phys. Rev. A: At., Mol., Opt. Phys.* **2010**, *81*, 043837.
(7) Zhou, Y.; Alam, M. Z.; Karimi, M.; Upham, J.; Reshef, O.; Liu, C.; Willner, A. E.; Boyd, R. W. Broadband frequency translation through time refraction in an epsilon-near-zero material. *Nat. Commun.* **2020**, *11*, 2180.
(8) Mendonça, J.; Guerreiro, A.; Martins, A. M. Quantum theory of time refraction. *Phys. Rev. A: At., Mol., Opt. Phys.* **2000**, *62*, 033805.
(9) Mendonça, J.; Guerreiro, A. Time refraction and the quantum properties of vacuum. *Phys. Rev. A: At., Mol., Opt. Phys.* **2005**, *72*, 063805.
(10) Yacomotti, A. M.; Raineri, F.; Cojocaru, C.; Monnier, P.; Levenson, J. A.; Raj, R. Nonadiabatic dynamics of the electromagnetic field and charge carriers in high-Q photonic crystal resonators. *Phys. Rev. Lett.* **2006**, *96*, 093901.
(11) Castellanos Muñoz, M.; Petrov, A. Y.; Eich, M. All-optical on-chip dynamic frequency conversion. *Appl. Phys. Lett.* **2012**, *101*, 141119.
(12) Kondo, K.; Baba, T. Dynamic wavelength conversion in copropagating slow-light pulses. *Phys. Rev. Lett.* **2014**, *112*, 223904.
(13) Gaafar, M. A.; Jalas, D.; O'Faolain, L.; Li, J.; Krauss, T. F.; Petrov, A. Y.; Eich, M. Reflection from a free carrier front via an intraband indirect photonic transition. *Nat. Commun.* **2018**, *9*, 1447.
(14) Beggs, D. M.; Krauss, T. F.; Kuipers, L.; Kampfrath, T. Ultrafast tilting of the dispersion of a photonic crystal and adiabatic spectral compression of light pulses. *Phys. Rev. Lett.* **2012**, *108*, 033902.
(15) Lee, K.; Son, J.; Park, J.; Kang, B.; Jeon, W.; Rotermund, F.; Min, B. Linear frequency conversion via sudden merging of meta-atoms in time-variant metasurfaces. *Nat. Photonics* **2018**, *12*, 765−773.
(16) Shcherbakov, M. R.; Werner, K.; Fan, Z.; Talisa, N.; Chowdhury, E.; Shvets, G. Photon acceleration and tunable

broadband harmonics generation in nonlinear time-dependent metasurfaces. *Nat. Commun.* **2019**, *10*, 1345.
(17) Dekker, R.; Driessen, A.; Wahlbrink, T.; Moormann, C.; Niehusmann, J.; Först, M. Ultrafast Kerr-induced all-optical wavelength conversion in silicon waveguides using 1.55 μm femtosecond pulses. *Opt. Express* **2006**, *14*, 8336−8346.
(18) Agrawal, G. P.; Baldeck, P.; Alfano, R. Temporal and spectral effects of cross-phase modulation on copropagating ultrashort pulses in optical fibers. *Phys. Rev. A: At., Mol., Opt. Phys.* **1989**, *40*, 5063−5072.
(19) Mehta, P.; Healy, N.; Day, T.; Badding, J. V.; Peacock, A. Ultrafast wavelength conversion via cross-phase modulation in hydrogenated amorphous silicon optical fibers. *Opt. Express* **2012**, *20*, 26110−26116.
(20) Bloembergen, N. Laser-induced electric breakdown in solids. *IEEE J. Quantum Electron.* **1974**, *10*, 375−386.
(21) Yablonovitch, E. Self-phase modulation of light in a laser-breakdown plasma. *Phys. Rev. Lett.* **1974**, *32*, 1101−1104.
(22) Wood, W. M.; Siders, C.; Downer, M. Measurement of femtosecond ionization dynamics of atmospheric density gases by spectral blueshifting. *Phys. Rev. Lett.* **1991**, *67*, 3523−3526.
(23) Lopes, N.; Figueira, G.; Dias, J.; Silva, L.; Mendonça, J.; Balcou, P.; Rey, G.; Stenz, C. Laser pulse frequency up-shifts by relativistic ionization fronts. *Europhys. Lett.* **2004**, *66*, 371−377.
(24) Fan, L.; Zou, C.-L.; Poot, M.; Cheng, R.; Guo, X.; Han, X.; Tang, H. X. Integrated optomechanical single-photon frequency shifter. *Nat. Photonics* **2016**, *10*, 766−770.
(25) Liberal, I.; Engheta, N. Near-zero refractive index photonics. *Nat. Photonics* **2017**, *11*, 149−158.
(26) Alam, M. Z.; De Leon, I.; Boyd, R. W. Large optical nonlinearity of indium tin oxide in its epsilon-near-zero region. *Science* **2016**, *352*, 795−797.
(27) Capretti, A.; Wang, Y.; Engheta, N.; Dal Negro, L. Enhanced third-harmonic generation in Si-compatible epsilon-near-zero indium tin oxide nanolayers. *Opt. Lett.* **2015**, *40*, 1500−1503.
(28) Caspani, L.; Kaipurath, R.; Clerici, M.; Ferrera, M.; Roger, T.; Kim, J.; Kinsey, N.; Pietrzyk, M.; Di Falco, A.; Shalaev, V. M.; et al. Enhanced nonlinear refractive index in ϵ-near-zero materials. *Phys. Rev. Lett.* **2016**, *116*, 233901.
(29) Reshef, O.; De Leon, I.; Alam, M. Z.; Boyd, R. W. Nonlinear optical effects in epsilon-near-zero media. *Nat. Rev. Mater.* **2019**, *4*, 535−551.
(30) Bruno, V.; Vezzoli, S.; DeVault, C.; Carnemolla, E.; Ferrera, M.; Boltasseva, A.; Shalaev, V. M.; Faccio, D.; Clerici, M. Broad frequency shift of parametric processes in Epsilon-Near-Zero time-varying media. *Appl. Sci.* **2020**, *10*, 1318.
(31) Alam, M. Z.; Schulz, S. A.; Upham, J.; De Leon, I.; Boyd, R. W. Large optical nonlinearity of nanoantennas coupled to an epsilon-near-zero material. *Nat. Photonics* **2018**, *12*, 79−83.
(32) Liu, C.; et al. Photon acceleration using a time-varying epsilon-near-zero metasurface. *ACS Photonics* **2021**, *8*, 716−720.
(33) Pang, K. et al. Plasmonic nanoantenna-enhanced adiabatic wavelength conversion using a time-varying epsilon-near-zero-based metasurface. In *Conference on Lasers and Electro-Optics*; 2020; paper FTh4Q.6.
(34) Smith, D. R.; Schultz, S.; Markoš, P.; Soukoulis, C. M. Determination of effective permittivity and permeability of metamaterials from reflection and transmission coefficients. *Phys. Rev. B: Condens. Matter Mater. Phys.* **2002**, *65*, 195104.
(35) Campione, S.; Brener, I.; Marquier, F. Theory of epsilon-near-zero modes in ultrathin films. *Phys. Rev. B: Condens. Matter Mater. Phys.* **2015**, *91*, 121408.
(36) Schulz, S. A.; Tahir, A. A.; Alam, M. Z.; Upham, J.; De Leon, I.; Boyd, R. W. Optical response of dipole antennas on an epsilon-near-zero substrate. *Phys. Rev. A: At., Mol., Opt. Phys.* **2016**, *93*, 063846.
(37) Vassant, S.; Hugonin, J.-P.; Marquier, F.; Greffet, J.-J. Berreman mode and epsilon near zero mode. *Opt. Express* **2012**, *20*, 23971−23977.
(38) Jun, Y. C.; Reno, J.; Ribaudo, T.; Shaner, E.; Greffet, J.-J.; Vassant, S.; Marquier, F.; Sinclair, M.; Brener, I. Epsilon-near-zero strong coupling in metamaterial-semiconductor hybrid structures. *Nano Lett.* **2013**, *13*, 5391−5396.
(39) Campione, S.; Wendt, J. R.; Keeler, G. A.; Luk, T. S. Near-infrared strong coupling between metamaterials and epsilon-near-zero modes in degenerately doped semiconductor nanolayers. *ACS Photonics* **2016**, *3*, 293−297.
(40) Bruno, V.; DeVault, C.; Vezzoli, S.; Kudyshev, Z.; Huq, T.; Mignuzzi, S.; Jacassi, A.; Saha, S.; Shah, Y.; Maier, S.; et al. Negative refraction in time-varying strongly coupled plasmonic-antenna−epsilon-near-zero systems. *Phys. Rev. Lett.* **2020**, *124*, 043902.
(41) Boyd, R. W.; Shi, Z.; De Leon, I. The third-order nonlinear optical susceptibility of gold. *Opt. Commun.* **2014**, *326*, 74−79.
(42) Guo, X.; Ding, Y.; Duan, Y.; Ni, X. Nonreciprocal metasurface with space−time phase modulation. *Light: Sci. Appl.* **2019**, *8*, 123.
(43) Abdelsalam, K.; Li, T.; Khurgin, J. B.; Fathpour, S. Linear isolators using wavelength conversion. *Optica* **2020**, *7*, 209−213.
(44) Jalas, D.; Petrov, A.; Eich, M.; Freude, W.; Fan, S.; Yu, Z.; Baets, R.; Popovic, M.; Melloni, A.; Joannopoulos, J. D.; et al. What is—and what is not—an optical isolator. *Nat. Photonics* **2013**, *7*, 579−582.

https://doi.org/10.1021/acs.nanolett.1c00550
Nano Lett. 2021, 21, 5907−5913